
Article:
West, NA orcid.org/0000-0002-3847-8478, Winner, JD, Bowersox, RDW et al. (1 more author) (2016) Resolving the energy and temperature dependence of C_6H_6 ∗ collisional relaxation via time-dependent bath temperature measurements. The Journal of Chemical Physics, 145 (1). ARTN: 014308. ISSN 0021-9606

https://doi.org/10.1063/1.4954896

The Journal of Chemical Physics

Resolving the energy and temperature dependence of $C_6H_6^*$ collisional relaxation via time-dependent bath temperature measurements

Cite as: J. Chem. Phys. **145**, 014308 (2016); https://doi.org/10.1063/1.4954896
Submitted: 22 April 2016 . Accepted: 15 June 2016 . Published Online: 06 July 2016

Niclas A. West, Joshua D. Winner, Rodney D. W. Bowersox, and Simon W. North

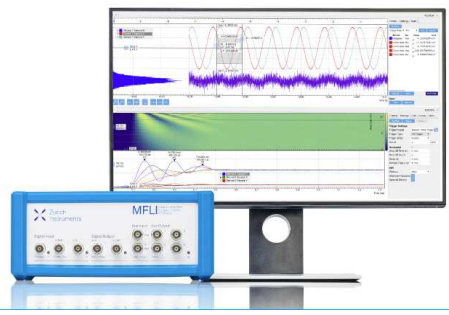

Resolving the energy and temperature dependence of $C_6H_6^*$ collisional relaxation via time-dependent bath temperature measurements

Niclas A. West,[1] Joshua D. Winner,[1] Rodney D. W. Bowersox,[2] and Simon W. North[1,a)]
[1]*Department of Chemistry, Texas A&M University, 3012 TAMU, College Station, Texas 77842, USA*
[2]*Department of Aerospace Engineering, Texas A&M University, 3141 TAMU, College Station, Texas 77842, USA*

(Received 22 April 2016; accepted 15 June 2016; published online 6 July 2016)

The relaxation of highly vibrationally excited benzene, generated by 193 nm laser excitation, was studied using the transient rotational-translational temperature rise of the N_2 bath, which was measured by proxy using two-line laser induced fluorescence of seeded NO. The resulting experimentally measured time-dependent N_2 temperature rises were modeled with MultiWell based simulations of Collisional Energy Transfer (CET) from benzene vibration to N_2 rotation-translation. We find that the average energy transferred in benzene deactivating collisions depends linearly on the internal energy of the excited benzene molecules and depends approximately linearly on the N_2 bath temperature between 300 K and 600 K. The results are consistent with experimental studies and classical trajectory calculations of CET in similar systems. *Published by AIP Publishing.* [http://dx.doi.org/10.1063/1.4954896]

I. INTRODUCTION

Understanding and modeling Collisional Energy Transfer (CET) of highly vibrationally excited molecules is important for predicting rate constants and product branching ratios for photoinitiated reactions, chemically activated processes, and reactions in high temperature combustion environments. In order to obtain quantitative kinetic predictions in these cases, modeling of energy transfer processes is necessary since rethermalization rates due to CET are comparable to chemical reaction rates. The treatment of such systems incorporates CET modeling through master equation simulations. Parameters for modeling the CET are often approximated from experiments and simulations of similar molecular systems which are often conducted in a limited to narrow range of conditions. There have been numerous studies on CET between highly vibrationally excited polyatomic molecules and various bath gases. Previous studies include highly vibrationally excited benzene,[1–3] deuterated and halogenated benzenes,[1,3–7] alkyl benzenes,[8] azulene,[9] naphthalene,[10] cycloheptatrienes,[11] and pyrazine[12] in a range of atomic and molecular baths including noble gases,[1] CO_2,[3–5,12,13] N_2,[6,7] and H_2O.[14]

The photophysics of highly vibrationally excited benzene has been the subject of numerous studies.[15–28] Absorption of a photon at 193 nm excites benzene to the S_2 ($^1B_{1u}$) state. The fluorescence quantum yield, triplet quantum yield, and dissociation rate are insignificant under the current experimental conditions, whereas highly vibrationally excited benzene is generated with a quantum yield near unity at 193 nm through internal conversion to benzene S_0. The time-dependent evolution of internal energy of non-reacting vibrationally excited aromatic molecules can be modeled using the master equation formulation,

$$\frac{dy(E',t)dE'}{dt} = \int_0^\infty [R(E',E)dE'y(E,t)]dE - \int_0^\infty [R(E,E')dE'y(E',t)]dE, \quad (1)$$

where $y(E',t)dE'$ is the concentration of molecules with energy between E' and $E'+dE'$ and $R(E,E')$ is the rate coefficient for (Vibration to N_2 Rotation-Translation) V-RT CET from an energy between E' and $E'+dE'$ to an energy between E and $E+dE$.[29,30] The energy transfer rate coefficients $R(E,E')$ can be expressed as

$$R(E,E')\,dE = \omega P(E,E')\,dE, \quad (2)$$

where ω is the total inelastic collision rate, $P(E,E')$ is the probability that a molecule initially at an energy between E' and $E'+dE'$ will transition to an energy between E and $E+dE$. The total inelastic collision rate can be approximated by the Lennard-Jones collision rate,

$$\omega = k_{coll} = \pi\sigma_{AB}^2 \langle v_r \rangle \Omega^{(2,2)^*} N, \quad (3)$$

where σ_{AB} is the Lennard-Jones diameter, $\langle v_r \rangle$ is the average relative speed, $\Omega^{(2,2)^*}$ is the collision integral, and N is the number density.[7,31]

Often a functional form is chosen for $P(E,E')$ to describe the energy transfer probability for collisions that transfer energy from the vibrationally excited molecule to the bath. Then, detailed balance, Equation (4), is utilized to determine $P(E',E)$, which describes the energy transfer probability for collisions that transfer energy from the bath to the vibrationally excited molecule,

$$\frac{P(E,E')}{P(E',E)} = \frac{\rho(E)}{\rho(E')} \exp\left(-\frac{E'-E}{k_BT}\right), \quad (4)$$

a)Author to whom correspondence should be addressed. Electronic mail: swnorth@tamu.edu. Fax: 979-845-2971.

where $\rho(E)$ is the benzene density of states at energy E, k_B is the Boltzmann constant, and T is the temperature in Kelvin. A generalized empirical function for $P(E,E')$ functions that have been used previously is a summation of exponential-down functions,

$$P(E,E') = \frac{1}{C(E')} \sum_{i=1}^{N} f_i \exp\left(-\left(\frac{E'-E}{\alpha_i(E')}\right)^{Y_i}\right), E' \geq E, \quad (5)$$

where $C(E')$ is a normalization constant, N is the total number of exponentials used, f_i is the fraction of each exponential such that the sum of the f_i values equals 1, $\alpha_i(E')$ is a fit parameter that is closely related to the average amount of energy transferred per collision, and Y_i is a parameter to weight more efficient collisions if $Y_i < 1$ or less efficient collisions if $Y_i > 1$. If Y_i is utilized in $P(E,E')$ (i.e., $Y_i \neq 1$), then Y_i is usually less than 1 for polyatomic-diatomic collisions and greater than 1 for polyatomic-polyatomic collisions at room temperature.[32] One simple functional form that can be utilized for the $P(E,E')$ down model is a single-exponential-down function where N = 1 and $Y_i = 1$. Although many studies model pressure-dependent reaction rate coefficients by utilizing an $\alpha_i(E')$ that is independent of internal energy, E', other studies that measure CET report an $\alpha_i(E')$ that has been modeled with a linear relationship with E',

$$\alpha_i(E') = C_0 + C_1 E', \quad (6)$$

where C_0 and C_1 are fit parameters.

The first evidence for an E′ dependent CET rate between a highly vibrationally excited aromatic molecule, azulene, and bath gases was observed in experiments by Barker *et al.*[33–35] Later, an E′ dependent benzene CET rate was reported in multiple experiments which monitored the internal energy of the photoexcited benzene during collisional relaxation. In UV Absorption (UVA) experiments carried out by Nakashima *et al.*, the authors measured changes in the transient absorption spectrum of photoexcited benzene and hexafluorobenzene due to CET in a N_2 bath.[16,36–40] Based on the experimental results, the authors proposed a single exponential decay function for the internal energy of the excited benzene over time implying that the CET rate depends on the internal energy of the excited benzene molecule.[16] In subsequent work, Barker and co-workers monitored infrared fluorescence (IRF) of photoexcited benzene as it collisionally relaxed in many bath gases, including N_2, and fit the experimental data with master equation modeling.[2,41] These experiments found that the CET from the excited benzene molecules depended linearly on average internal energy of benzene over a large energy range.

There have been several experiments and calculations examining energy exchanged in single collisions between single energy-donor molecules and single bath molecules which have also found that CET efficiency depends on the energy-donor molecule internal energy. In one study, Lenzer *et al.* employed single-interaction classical trajectory calculations of benzene and hexafluorobenzene, initiated at various vibrational and rotational excitations, colliding with a variety of rare gases.[1] The authors observed that the energy transferred per collision depended approximately linearly on the level of vibrational excitation of benzene. They also found donor rotational energy to transfer more effectively at higher rotational energy of the donor molecules and to be very small when the donor rotational temperature was close to the bath temperature. In related experiments with excited pyrazine in a CO_2 bath, energy transfer to both rotational and translational energies of the bath increased as the initial internal energy of the pyrazine increased from laser excitation at 308.8 nm (32 383 cm^{-1}) to laser excitation at 266 nm (37 594 cm^{-1}).[13]

Another method that has been utilized to measure the CET rate dependence on E' is Kinetically Controlled Selective Ionization (KCSI). CET rate data from KCSI experiments are preferred over UVA and IRF experiments due to the precision of KCSI measurements as discussed by Barker *et al.*[31] In KCSI experiments performed by Lenzer *et al.* on a variety of highly vibrationally excited molecules, the authors resonantly ionized the vibrationally excited molecules within narrow energy windows at varying time delays after the generation of the excited molecules such that collision-dependent internal energy distribution profiles could be obtained.[42–44] The authors suggested that CET efficiency could be roughly modeled utilizing a single exponential-down function, N = 1 and $Y_i = 1$ in Equation (5), with a $\alpha_1(E')$ that is linearly dependent on E', but that an exponential-down model utilizing more parameters, N ≠ 1 and $Y_i \neq 1$ in Equation (5), is preferred if more accurate CET distribution fits are available for the system under study.

When more data on the post-collision internal energy distributions of a vibrationally excited aromatic molecule and a bath gas are available, $P(E,E')$ are often fit to a biexponential-down function, N = 2 and $Y_i = 1$ in Equation (5), instead of a single-exponential-down function. Utilizing a biexponential-down function allows for the inclusion of a small fraction (usually $f_2 < 0.10$) of supercollisions, collisions that transfer an average of >2000 cm^{-1}. Supercollisions were first discovered in a number of experimental and theoretical studies.[45–56] Supercollisions are described by the second exponential in $P(E,E')$ such that $\alpha_1(E') \ll \alpha_2(E')$, and the energy dependence of $\alpha_1(E')$ and $\alpha_2(E')$ have been experimentally and theoretically fit for a limited energy range for a limited number of systems.

Early work to measure the high energy tail of the biexponential $P(E,E')$ for C_6H_6 was carried out by Flynn and co-workers, who investigated the single collision V-RT CET behavior of photoexcited C_6H_6, C_6D_6, and C_6F_6 colliding with CO_2 by probing CO_2 via Tunable Diode Laser Absorption Spectroscopy (TDLAS).[3,5] The work revealed a small fraction of supercollisions occurring in CO_2 collisions with nascent highly excited benzene molecules. These findings are consistent with the findings of Lenzer *et al.* who employed single-interaction classical trajectory calculations of benzene and hexafluorobenzene initiated at various vibrational and rotational excitations colliding with rare gases, and utilized a bi-exponential function for a P_{down} model when fitting changes in internal energy of the excited benzene and hexafluorobenzene.[1] Additionally, in KCSI work by Lenzer *et al.*, biexponential-down and parametric ($Y_i \neq 1$) exponential-down models were used.[42–44]

The dynamics of supercollisions has also been the focus of numerous studies. Clary *et al.* employed vibrational close-coupling infinite order sudden quantum scattering calculations

for highly vibrationally excited benzene colliding with rare gases.[57] In this treatment, up to two vibrational modes of a benzene molecule are excited in each simulation and the rotation is fixed. Then an ensemble of calculations was run in order to average over all orientations such that an approximation of a full quantum treatment of the collision complex could be achieved. The authors found that an increase in inelastic cross section occurs with an increase in excitation of low-frequency out-of-plane vibrational modes. These highly excited out-of-plane vibrations are thought to be the origin of supercollisions in benzene molecules. The dynamics of benzene supercollisions was also probed experimentally by Mitchell *et al.* who studied highly excited difluorobenzene isomers colliding with CO_2 by probing CO_2 TDLAS after a single collision.[4] They observed a correlation of the ν_{11} and ν_{16} vibrational modes, the "gateway" modes, with more efficient energy transfer.

Models utilizing a single exponential $P(E,E')$ can be compared to models utilizing a biexponential $P(E,E')$ by calculating the first two moments of the internal energy distribution of a species simulated with a master equation treatment,[58]

$$\langle \Delta E(E')^n \rangle = \int_0^\infty (E - E')^n P(E,E') dE, \tag{7}$$

where n is the moment number of the internal energy distribution. Although both single and biexponential $P(E,E')$ models can be tuned to yield the same first moment of the internal energy distribution, $\langle \Delta E \rangle$, the second moment of the internal energy distribution, $\langle \Delta E^2 \rangle$, will be larger when utilizing the biexponential $P(E,E')$ model.[43,59] A larger $\langle \Delta E^2 \rangle$ value is significant in reacting systems in which either a larger fraction of reactants would be quickly collisionally deactivated in the case of a photochemical reaction, or a larger fraction of reactants would be quickly activated in the case of a thermal reaction. Therefore the biexponential $P(E,E')$ model results in slower or faster reaction rates than the single exponential $P(E,E')$ model depending on the initial internal energy of the reactants.

The first two moments of the collisional relaxation of hexafluorobenzene and "model" benzene were calculated in recent work by Paul *et al.*[6,7] There the authors performed classical trajectory calculations of single highly vibrationally excited C_6F_6 or "model" C_6H_6 molecule in constant density periodic baths of N_2 to simulate the time dependent deactivation of the excited molecule. The large variation in the second moment of the CET was shown to not have a significant effect on the overall relaxation rate of the highly vibrationally excited molecule.

Another quantity that is often reported for many systems in studies utilizing a master equation treatment as well as in CET studies is the average energy transferred in deactivating collisions,[31,58]

$$\langle \Delta E_d \rangle = \frac{\int_0^{E'} (E' - E) P(E,E') dE}{\int_0^{E'} P(E,E') dE}. \tag{8}$$

There have been conflicting reports of the dependence of $\langle \Delta E_d \rangle$ on bath temperature for benzene and related aromatic species. Barker *et al.* have reported that, in experimentally measured (KCSI and IRF) polyatomic energy-donor molecules in diatomic and monatomic baths, there is a very little dependence of CET on bath temperature when measured near room temperature.[31] However, a different temperature dependence model was proposed by Miller *et al.*, who utilized a multiple well master equation approach to study the temperature dependence of energy transfer, first in methane-Ar collisions, and later in propargyl recombination to form benzene between 300 and 2000 K.[58,60] In order to fit recombination rate constants, the form of their average energy transferred in deactivating collisions is related to bath temperature through the relation $\langle \Delta E_d \rangle = 400(T/300)^{0.7}\,cm^{-1}$. Yet another study of benzene CET rate dependence on bath temperature was carried out by Bernshtein and Oref. They performed classical trajectory calculations of highly vibrationally excited benzene colliding with unexcited benzene and argon molecules at 100, 200, 300, and 500 K.[32] It was found that $\langle \Delta E_d \rangle$ in excited benzene-argon collisions increases between 100 and 500 K, but that $\langle \Delta E \rangle$ remains approximately constant.

In this paper, we present experimental time-dependent rotation-translation temperature data for a N_2 bath as a means of studying $C_6F_6^*$ –N_2 V-RT CET. Although the current measurements are only sensitive to the rotational and translational modes of the bath, a near unity fraction of the CET is predicted to flow from benzene vibration to bath rotation and translation. We therefore equate the resulting energy loss of excited benzene in MultiWell master equation simulations with the energy gain of the bath RT modes.[29,30] This way integrating the bath heat capacity to the time-dependent bath energy yields bath temperatures that are directly comparable to the experimental time-dependent temperature rises. The results have been modeled using MultiWell master equation to describe the internal energy and bath temperature dependence of CET from highly vibrationally excited benzene to the N_2 bath. The bath temperature range studied was 300–600 K and the initial internal energy was a 300 K thermal vibrational distribution shifted by 51 813 cm^{-1} which collisionally rethermalized on the time scale of the experiment.

II. EXPERIMENTAL METHODS

Experiments to measure the bath temperature rise due to collisional energy transfer (CET) from highly vibrationally excited benzene ($C_6H_6^*$) were performed in a custom-built slow-flow cell shown in Figure 1.

The gas mixture was prepared by mixing a constant ratio of NO gas and N_2 gas just prior to passing the gas through a high pressure bubbler with benzene. The mixture of certified 5% NO in N_2 (Matheson) and 99.99% N_2 (Praxair) was maintained at a constant pressure of around 137.9 kPa by a LabVIEW Proportional-Integral-Derivative (PID) algorithm. The PID algorithm monitored by the pressure-dependent DC voltage output of a pressure transducer (Omega Type PX309-200A5V) with a range of 1379 kPa and generated a pressure dependent DC voltage output to control mass flow controllers (MKS Mass-Flo 1179A) driven by a four-channel power supply/readout (MKS 247) operated in constant-flow-ratio

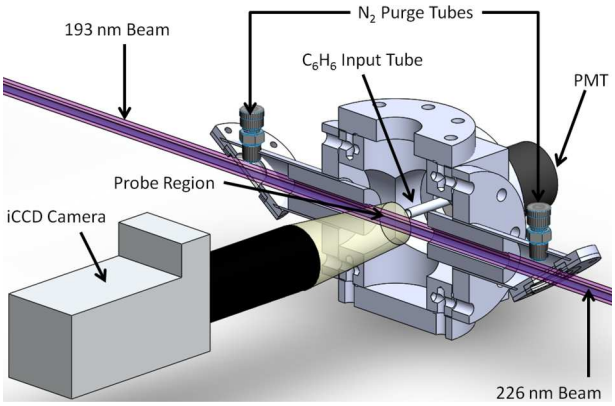

FIG. 1. Schematic diagram of slow-flow cell.

mode. The NO/N_2 gas was passed through a custom-built high pressure bubbler containing benzene (C_6H_6) (99.8%, Sigma-Aldrich). The resulting mixture was then passed through a custom built water cooled 7.5 m stainless steel coil, which maintained a constant partial pressure of C_6H_6. The water was maintained at a constant temperature which was adjusted between 6.5 and 13.5 °C by a refrigerated circulating bath (Cole-Parmer Type Polystat 12102-00) yielding a partial pressure of 5–7 kPa of C_6H_6 (1%–7% of the gas mixture) calculated using the known vapor pressure of C_6H_6.

Reactant gases were introduced into the cell by mass flow controllers (MKS Mass-Flo 1179A) driven by a four-channel power supply/readout (MKS 247) operated in constant-flow mode. One mass flow controller introduced the C_6H_6 gas mixture into the cell, and another mass flow controller introduced N_2 through the window purge lines of the cell. Prior to each experiment, the cell windows were treated with a UV/ozone cleaner (BioForce Nanosciences Type ProCleaner 110) for 30 min to reduce C_6H_6 adsorption and burning onto the windows. The cell was pumped down by a Leybold D65B backing pump and Ruvac WS1001US Roots blower system establishing a slow flow system to insure that reactant gas was refreshed between every laser shot. Pressure in the cell was monitored by a pressure transducer (Baratron MKS Type 622) with a range of 13.3 kPa.

Highly vibrationally excited benzene ($C_6H_6^*$) was generated by excitation at 193 nm using the ArF output of an excimer laser (Lambda Physik COMPex 201) operating at 10 Hz. Based on the absorption cross section of C_6H_6 of 1.8×10^{-17} cm^2 at 193.1 nm and the laser fluences employed, fractional excitations of approximately 0.1–0.3 were achieved within the beam volume.[61,62]

The bath time-dependent rotational-translational temperature was measured via laser induced fluorescence (LIF) using the $A^2\Sigma^+$ (v′ = 0) ← $X^2\Pi_{1/2}$ (v″ = 0) transition near 226 nm. The 226 nm probe beam (7 × 2 mm) was generated by the frequency doubled tunable output of a Sirah Cobra CBR-G-18 pulsed dye laser using coumarin 450 in methanol. The dye laser was pumped by the 355 nm third harmonic of a Spectra Physics LAB-150-10 Nd:YAG laser operating at 10 Hz. The 226 nm pulses had typical durations of 10 ns, linewidth of 0.08 cm^{-1}, and exit power of 2 mJ/pulse (2×10^5 W). The 193 nm pump beam and 226 nm probe beam were collinearly aligned through the cell. The delay between the pump and probe lasers was varied by a digital delay generator (BNC, Model 565).

Fluorescence images were acquired with an Andor iStar DH734 ICCD camera situated perpendicular to the pump and probe beams. A −10 °C CCD temperature was maintained by the camera's internal thermoelectric cooler which was cooled with 21 °C water maintained by a refrigerated circulating bath (Neslab Type CFT-25). The fluorescence was focused onto the camera with a UKA 105 mm F = 4 : 0 UV lens mounted on extension rings. To reduce contributions from background light in the room, a UG5 visible filter (Thorlabs) was mounted to the front of the lens, providing a band-pass filter for light near 240–395 nm. During acquisition, iCCD pixels were binned to obtain 16 pixel × 32 pixel images on the camera yielding an image spatial resolution of 0.985 mm/pixel × 1.970 mm/pixel (V × H). Image signals were integrated on the CCD for 1–10 laser shots.

The NO LIF signal was determined to be in the linear regime with respect to 226 nm laser power by attenuating the 226 nm beam with successive additions of fused silica windows into the beam path and fitting the NO LIF intensity vs 226 nm beam power. Shot-to-shot 226 nm laser power fluctuations were also monitored by directing scattered light from the 226 nm beam onto a phosphor plate (Type P46) and measuring the phosphorescence with a PMT (Hamamatsu Type H6780-03). To remove room light, a UG5 visible filter (Thorlabs) was mounted to the phosphor plate, and to remove light besides phosphorescence, a 546.1 nm band pass filter (Omega Optical Type 546.1BP10) was mounted to the PMT. The PMT signal was then digitized by a 12-bit Lecroy (HRO 66Zi) oscilloscope at a sampling rate of 2 GS/s and integrated using a custom LabVIEW program. The resulting phosphorescence signal was integrated with a 1000 ns gate. Due to the linear dependence of NO LIF on 226 nm power, variation in NO LIF signal due to shot-to-shot fluctuations in 226 nm laser power were corrected by dividing LIF signal by the integrated power-correction phosphorescence signal.

NO two-line Planar Laser Induced Fluorescence (PLIF) temperatures were determined utilizing the Q_2+ R_{12} (5.5) and P_2+ Q_{12} (17.5) transitions $A^2\Sigma^+$ (v′ = 0) ← $X^2\Pi_{1/2}$ (v″ = 0) band, due to their large S/N and temperature sensitivity between 300 K and 700 K. Bath temperatures were evaluated with the following equation:

$$\frac{S_1}{S_2} = C_{12} \exp\left(-\frac{\Delta E_{21}}{k_B T_{rot}}\right), \tag{9}$$

where S_1 and S_2 are the integrated fluorescence signals, ΔE_{21} is the difference in rotational energy between the probed rotational states, k_B is the Boltzmann constant, T_{rot} is the NO rotational-translational temperature in Kelvin, and C_{12} accounts for the stimulated absorption coefficients, the wavelength dependence of the laser intensity, the fluorescence quantum yield, and the efficiency of the collection optics and camera. C_{12} was determined by measuring the fluorescence intensities of the bath at room temperature. Two line temperature values were also checked by scanning the 226.5 -226.7 nm NO LIF region and performing least-squares fits to simulations in LIFBASE for scans between 300 K and

700 K.[63] The scans also demonstrated that the system was thermalized at the measured pump-probe delays.

We observed that >95% of the short term temperature rise occurred by 4 μs after the pump beam, and a plot of the temperature map of the maximum temperature achieved in the bath at 4–6 μs shows that there was a large gradient in bath temperature in the region imaged by the camera. This temperature gradient was due to attenuation of 193 nm light by C_6H_6 as well as a gradient of C_6H_6 partial pressure in the region examined. However, diffusion of $C_6H_6^*$ was calculated to be between 10 and 20 μm/μs and only significantly affected temperature measurements between 10 and 15 μs.

III. RESULTS AND DISCUSSION

A. Experimental results

Spatially resolved two-line NO PLIF temperature measurements were made for each pixel location in the raw fluorescence images. Representative raw emission images at a pump-probe time delay of 0.2 μs are shown in Figure 2. Each image was acquired >10 times and was averaged to improve the S/N. In these images, the 226 nm probe beam was directed right-to-left and the 193 nm beam was directed left-to-right. The horizontal variation of Q_2 (5.5) NO fluorescence is due to quenching by C_6H_6, resulting in the lowest signal near the exit of the 6.35 mm tube where the $C_6H_6/N_2/NO$ mixture was introduced into the slow-flow cell, the location in which [C_6H_6] was largest. For the smallest pump-probe time delays, we observed appreciable emission from C_6H_6 on the left side of the images, Figure 2, due to a larger 193 nm beam power in that region. The variation from left to right is consistent with the attenuation of 193 nm beam power due to C_6H_6 absorption. For the smallest pump-probe time delay images, up to 33% of the signal for pixels on the left to right side of the image came from benzene emission. Therefore, at each pump-probe time delay, 10 images with the 226 nm beam blocked were acquired, averaged, and subtracted from the NO fluorescence (226 nm beam on) images.

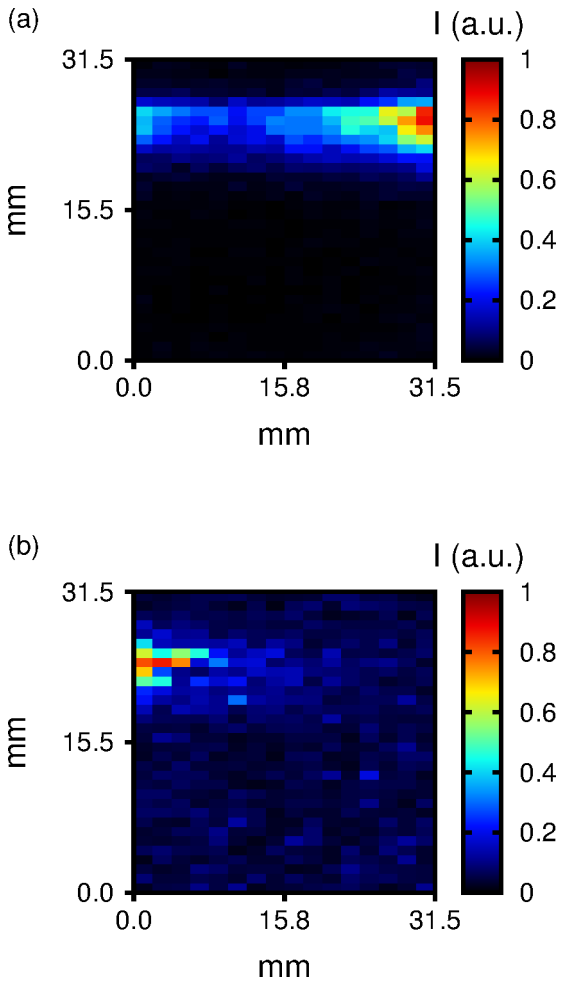

FIG. 2. Raw images at 18 Torr at a pump-probe time delay of 0.2 μs. (a) Q_2 (5.5) NO fluorescence, (b) C_6H_6 emission from 193 nm excitation (226 nm laser blocked).

Following subtraction of 193 nm emission, each temperature value was calculated with Equation (9) by comparing single pixel integrated signals, S_1 and S_2, originating from the same pixel position in a pair of images. The image that yielded S_1 probed the J = 5.5 rotational state of NO and the image that yielded S_2 probed the J = 17.5 rotational state of NO. These image pairs were acquired at each pump-probe time delay in a randomized order to yield a time-dependent temperature rise for each pixel. The experiment was then repeated >10 times to yield a group of >10 temperature rises for each pixel such that temperature rise averaging and analysis of statistical error could be carried out for each pixel location.

Each group of >10 temperature rises at each pixel location was scaled and averaged to yield an improved S/N temperature rise at each pixel location. Scaling of the >10 temperature rises at each pixel location to the same final temperature was carried out to insure that the error bars in time-dependent temperature values originate from statistical fluctuations in temperature measurements and not small differences in final temperature from one experiment to the next. To scale the group of temperature rises at each pixel location, each group was first denoted by an integer k. Each temperature rise within a group was then denoted by an integer j. Next, each time-dependent temperature value was denoted by $T_{ijk}(t)$ where i represents each sequential pump-probe time delay. Then, the final average temperature, $\langle T_{fjk}\rangle$, for each temperature rise was determined by averaging the $T_{ijk}(t)$ values at pump-probe time delays between 3 and 6 μs of that rise,

$$\langle T_{fjk}\rangle = \sum_{i=I-N_f}^{I} \frac{T_{ijk}(t)}{N_f}, \tag{10}$$

where I is the total number of pump-probe time delays and N_f is the number of final $T_{ijk}(t)$ values to be averaged. The pump-probe delay of 6 μs was chosen as the cutoff for analysis purposes because after 6 μs, factors like diffusion caused temperature from each pixel location to either slightly increase or decrease depending on if the surrounding gas was either higher or lower in temperature on average. Next, the average of the $\langle T_{fjk}\rangle$ values, $\langle\langle T_{fk}\rangle\rangle$, was determined for each group in order to determine the final temperature to which the rises should be scaled,

$$\langle\langle T_{fk}\rangle\rangle = \sum_{j=1}^{J_k} \frac{\langle T_{fjk}\rangle}{J_k}, \tag{11}$$

where J_k is the total number of temperature rises in group k. Next, all $T_{ijk}(t)$ values were scaled utilizing Equation (12),

$$T'_{ijk}(t) = (T_{ijk}(t) - T_0)\left[\frac{(\langle\langle T_{fk}\rangle\rangle - T_0)}{(\langle T_{fjk}\rangle - T_0)}\right] + T_0, \tag{12}$$

where $T_0 = 300$ K in this experiment. At this point, all temperature rises within each group have been scaled to the same final average temperature, $\langle\langle T_{fk}\rangle\rangle$. Next the final scaled and averaged temperature rise for each group was calculated by averaging the scaled time-dependent temperature values from each time delay.

$$\langle T'_{ik}(t)\rangle = \sum_{j=1}^{J_k} \frac{T'_{ijk}(t)}{J_k}. \tag{13}$$

Temperature error bars for the scaled and averaged temperature rises were then determined from the standard deviation, σ_{ik}, of the scaled time-dependent temperature values at each time delay,

$$\sigma_{ik} = \sqrt{\frac{1}{J_k}\sum_{j=1}^{J_k}\left(T'_{ijk}(t) - \langle T'_{ik}(t)\rangle\right)^2}. \tag{14}$$

The result was an averaged temperature rise for each pixel location in the field of view in the raw image. The final average temperature, $\langle T_{fk}\rangle$, at each pixel location varied from 350 to 700 K within the field of view as shown in Figure 3. The gradient in final average temperature occurred due to a gradient in benzene concentration as well as a gradient in 193 nm beam power. The temperature gradient in the probed region allowed for the study of the temperature dependence of the CET efficiency.

Since a dependence of CET efficiency on bath temperature was expected, the averaged temperature rise of each pixel was placed into a temperature dependent bin based on the final average temperature, $\langle\langle T_{fk}\rangle\rangle$. The bins were separated according to final average temperature every 30 K. A number of pixels had large error bar temperature measurements which originated from regions with low NO fluorescence signal due to low 226 nm beam power at the edges of the beam. Temperature rises with undesirably large error bars were rejected from the bins if, in that temperature rise, the average of the error bars was larger than 20% of the total rise in temperature. Each bin of averaged temperature rises was then scaled and averaged using the same procedure that groups of temperature rises from each pixel location were scaled and averaged. This yielded time-dependent temperature rises which could be examined for their CET rate dependence on the final temperature of the rise. Therefore the CET efficiency in a final scaled and averaged temperature rise of a bin represents the average CET efficiency for the range of temperature rises to different final temperatures that were averaged in that bin.

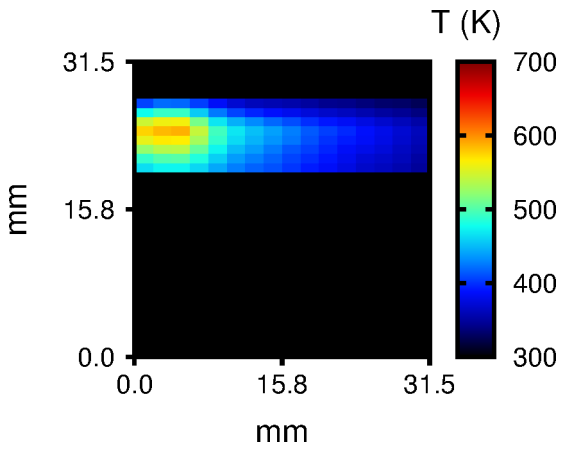

FIG. 3. Spatially resolved average temperature between 3 and 6 μs pump-probe time delay.

The time-dependent temperature rises were then converted to collision-dependent temperature rises for direct comparison with previous CET studies. To accomplish this, the time between successive temperature measurements was converted to number of collisions using the temperature dependent collision rate, Equation (3). The temperature used to calculate the collision rate was the average of successive temperature values. For collision rate calculations, the empirical collision integral, $\Omega^{(2,2)^*}$, was taken to be

$$\Omega^{(2,2)^*} = \frac{A}{(T^*)^B} + \frac{C}{e^{DT^*}} + \frac{E}{e^{FT^*}}, \tag{15}$$

where $T^* = k_B T/\epsilon_{AB}$, $A = 1.161\,45$, $B = 0.148\,74$, $C = 0.524\,87$, $D = 0.773\,20$, $E = 2.161\,78$, $F = 2.437\,87$, k_B is the Boltzmann constant, and ϵ_{AB} is the Lennard-Jones well depth.[64] Lennard-Jones parameters, $\sigma_{AB} = 4.6$ Å and $\varepsilon_{AB}/k_B = 181.3$ K, were calculated utilizing Lennard-Jones parameter combination rules with C_6H_6 and N_2 Lennard-Jones parameters.[65] The Lennard-Jones collision rate model was used in this study for better comparison to trajectory calculations, even though it is known that the inelastic collision rate is higher than the Lennard-Jones collision rate at high vibrational density of states and lower at low vibrational density of states.[31,57] Since the energy transfer rate is determined by both the inelastic collision rate and the probability of energy transfer function, our derived parameters for the probability of energy transfer function are only valid when using the Lennard-Jones collision rate.[31]

B. MultiWell modeling

The collisional relaxation of $C_6H_6^*$ in a N_2 bath was modeled using the master equation formulation in the program MultiWell.[29,30] The active K-rotor and the adiabatic 2-D rotor model was utilized in the calculation of $C_6H_6^*$ density of states. All energy transfer parameters derived in this paper are only applicable to this model since the density of states is used in the detailed balance calculation which changes the internal energy dependence of the CET rate. Exact counts of the densities of states were carried out with the Stein-Rabinovitch extension[66] of the Beyer-Swinehart algorithm.[67] The utilized C_6H_6 vibrational frequencies were obtained from Lenzer *et al.*[1] The utilized C_6H_6 rotational moments of inertia, $I_A = 177.8$ amu Å and $I_B = I_C = 88.9$ amu Å, were obtained from Herzberg.[68] A single exponential form of $P(E, E')$, $N = 1$ and $Y_1 = 1$ in Equation (5), was used since the temperature rise experiment

was insensitive to the contribution of supercollisions to CET. However, when a large amount of energy is transferred into bath molecule rotational energy in a single collision, it is possible to form a high energy metastable rotational state that may not thermalize on the same time scale as the rest of the bath.[69] Therefore, it is possible that the temperature rises measured in this study underrepresent the total energy transferred from the excited benzene to the bath rotational energy.

In order to generate fits to experimental temperature rises, the simulated MultiWell plots of ensemble average benzene internal energy versus number of collisions were converted to simulated temperature rises. Since previous studies of similar systems report predominantly V-RT CET and very little V-V CET to the bath, the energy lost from benzene was transferred evenly into N_2 rotation and translation in the simulation.[7] To obtain N_2 temperature values, the N_2 translational, rotational, and vibrational heat capacities were integrated to the temperatures that yielded the N_2 internal energies determined by the simulation, although the integrated vibrational heat capacity comprised <1% of the N_2 total energy between 300 and 700 K.

It is possible that there is a non-negligible contribution from $C_6H_6^*$–C_6H_6 CET in our experiments. However, we expect this to be a slower path for CET to the bath rotation-translation modes since the pathway involves predominantly V-V CET, redistributing vibration from highly excited benzene to vibration in unexcited benzene.[31,32] As a result, both benzenes in the $C_6H_6^*$–C_6H_6 collision would later undergo V-RT CET to the bath at slower rates than the highly excited benzene would have undergone if the highly excited benzene had not collided with an unexcited benzene. Inefficient $C_6H_6^*$–C_6H_6 V-RT collisions also occur, $\langle \Delta E \rangle$ of about -17 cm^{-1} for V-R CET at E' of 40 700 cm^{-1} in classical trajectory calculations by Bernshtein and Oref, which would quickly RT-RT CET to the N_2 bath.[32] However, the effect of both $C_6H_6^*$–C_6H_6 CET pathways for CET to the bath in our experiment is also diminished by $C_6H_6^*$–C_6H_6 collisions occurring much less frequently than $C_6H_6^*$–N_2 collisions. Utilizing Equation (3), the collision rate for $C_6H_6^*$–N_2 collisions at 18 Torr decreases from 2.7×10^8 s^{-1} to 1.4×10^8 s^{-1} between 300 K and 700 K. Whereas the collision rate for $C_6H_6^*$–C_6H_6 collisions at 1.26 Torr (7% of 18 Torr) decreases from 2.8×10^7 s^{-1} to 1.2×10^7 s^{-1} between 300 K and 700 K. Therefore the $C_6H_6^*$–N_2 collision rate is consistently at least a factor of 9 larger than the $C_6H_6^*$–C_6H_6 collision rate in this experiment which implies that the effect of the large magnitude $C_6H_6^*$–C_6H_6 collisions on the overall CET rate observed in the temperature rises is greatly diminished. Therefore, any CET rate parameters derived from these data are for a gas mixture and not pure $C_6H_6^*$–N_2 collisions. However, improvements in this method such as higher probe laser power, better iCCD cameras, and an improved slow-flow cell will make it possible to use smaller C_6H_6 mixing ratios which will significantly reduce the effect of $C_6H_6^*$–C_6H_6 collisions on the overall CET rate observed in the temperature rises.

In our initial treatment of CET, we employed a constant value for $\alpha_1(E')$ in $P(E',E)$ (Equation (5)) which was optimized to yield best a fit temperature rise simulation. The model utilizing a constant value for $\alpha_1(E')$ implies that a constant amount of energy is transferred in deactivating collisions, $\langle \Delta E_d \rangle$, which yields a linear temperature rise that curves to an asymptote value as benzene thermalizes, as seen in Figure 4. The best overall fit to the 12 Torr data with a ΔT of 130 K is shown in Figure 4. The curvature in the experimental temperature rise data is inconsistent with a master equation model utilizing a constant $\alpha_1(E')$ because the model underestimates the early CET rate and overestimates the late CET rate of the temperature rise. The curvature in the temperature rise suggests a dependence of the CET rate on temperature, $\langle E' \rangle$, or both.

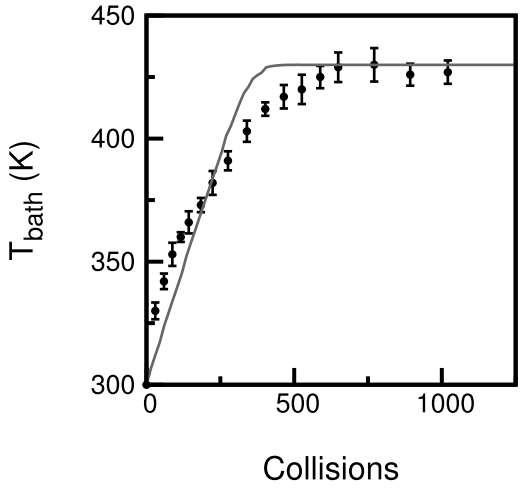

FIG. 4. Temperature rise at 12 Torr with $\Delta T = 130$ K (black circles) compared to a master equation simulation using a best fit constant $\alpha_1(E')$ of 275 cm^{-1} (grey line). Error bars represent ±1 σ statistical error only.

In order to assess the possibility that the curvature in the experimental temperature rise was the result of a bath temperature dependent CET rate, we calculated the difference between subsequent temperature values in Figure 4 which we converted into $-\langle \Delta E \rangle$ values and plotted versus the corresponding average of the subsequent temperature values as shown in Figure 5. If the change in CET rate were to depend only on the bath temperature, then the values of $\alpha_1(E')$ would have to be inversely proportional to temperature. However,

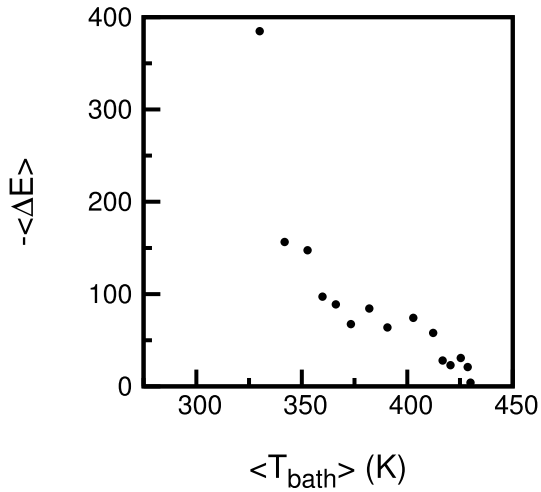

FIG. 5. Change in benzene internal energy per collision vs average temperature for a temperature-binned temperature rise.

this trend is counter to the temperature dependence on V-RT energy transfer utilized in most models which often utilize CET parameters that are approximately linearly increasing with increase in temperaure.[32,58,60]

An alternate origin for the observed curvature in a temperature rise is a form for $\alpha_1(E')$ that is linearly dependent on E', Equation (6). The temperature rise from the linearly dependent $\alpha_1(E')$ simulation was found to be a good fit to the experimental temperature rise at 12 Torr, as seen in Figure 6. Furthermore, identical C_0 and C_1 parameters are found for the linearly dependent $\alpha_1(E')$ for both the 12 Torr and 18 Torr experimental temperature rises, once converted to collision space. This result confirms that the energy transfer per collision is also independent of pressure as expected.

In order to visualize how the CET efficiency varies as a function of benzene internal energy, we plot the average energy transferred per collision, $\langle \Delta E \rangle$, versus $\langle E' \rangle$ in Figure 7. This figure was generated from the optimized simulations of Figures 4 and 6 by taking the average change in energy of benzene per collision and plotting it versus the average internal energy of benzene every 20 collisions. When comparing the

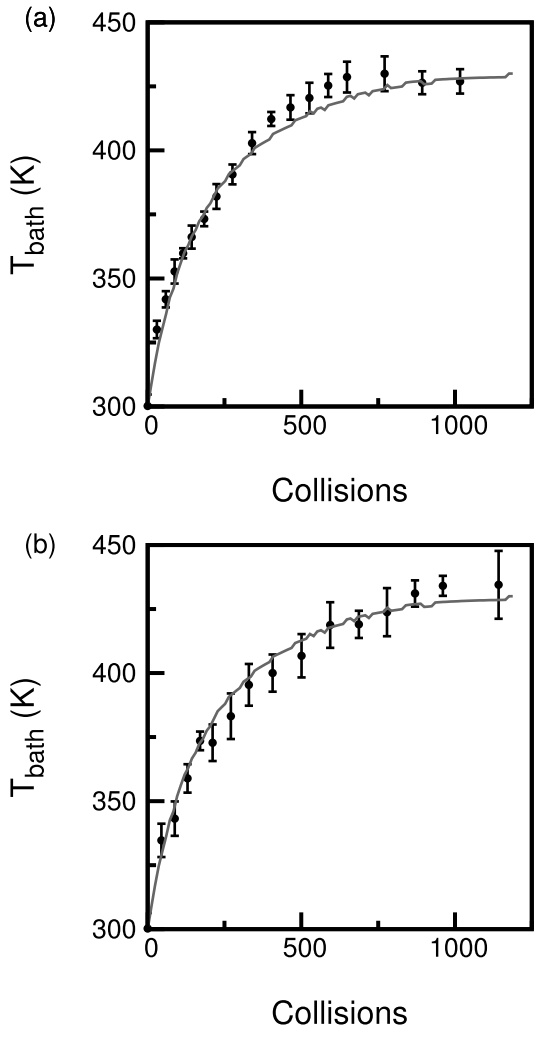

FIG. 6. Experimental temperature-binned temperature rises (black circles) at two pressures. (a) 12 Torr. (b) 18 Torr. These rises were simultaneously modeled (grey lines) using $C_0 = 138$ cm^{-1} and $C_1 = 0.0082$ in Equation (5). Error bars represent ±1 σ statistical error only.

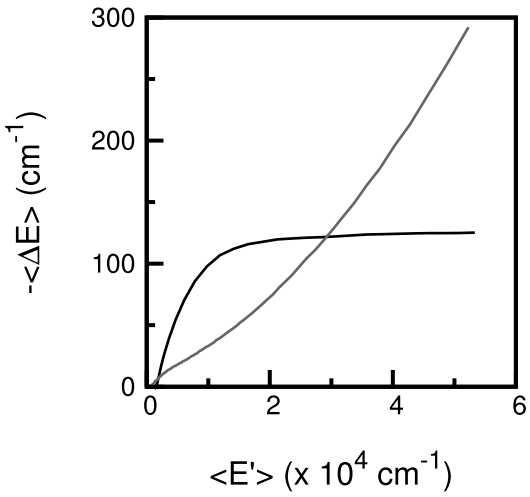

FIG. 7. Models utilizing constant (black line) and linear (grey line) forms of $\alpha_1(E')$ in Equation (5).

average energy transferred per collision, $\langle \Delta E \rangle$ in Equation (7), between a constant $\alpha_1(E')$ model and an energy dependent $\alpha_1(E')$ model in Figure 7, the energy transfer is initially much larger for the energy dependent $\alpha_1(E')$ until $\langle E' \rangle$ = 30 000 cm^{-1} where the constant $\alpha_1(E')$ model overtakes the linear model. It should be noted that for the constant $\alpha_1(E')$ simulation, the deviation from linearity at low values of $\langle E' \rangle$ is a result of detailed balancing, where the probability of an activating collision has risen sufficiently to impact the average energy transferred per collision.

It is of importance to examine the temperature dependence of CET, as there is still uncertainty in this area.[31] We observe that the optimized simulations of time-dependent temperature rises corresponding to different final ΔT require fit parameters of Equation (5) that depend on the average final temperature. Table I summarizes the optimized fit parameters using Equation (5) of the linear $\alpha_1(E')$ that were fit utilizing least squares analysis for several different temperature rises. The optimized values of both C_0 and C_1 increase approximately monotonically with temperature, indicating a positive correlation of CET efficiency with temperature. The increase of C_0 and C_1 between ΔT of 130 K–310 K results in a 59% increase in $\alpha_1(E')$ for an initial E' value of 53 326 cm^{-1}. In order to assess the error bars for the C_0 and C_1 parameters the least squares of the fits to the temperature rises versus changes in C_0 and C_1 were examined. For all of the least squares plots, there was noise at

TABLE I. Parameters for Equation (6) from fitting model temperature rise data to experimental temperature rises of differing total change in temperature.

ΔT (K)	C_0 (cm^{-1})	C_1 (unitless)	$\alpha_1(E')$ (cm^{-1})
130	138 ± 12	0.0082 ± 0.0007	575 ± 27
155	162 ± 5	0.0079 ± 0.0010	583 ± 20
185	162 ± 7	0.0091 ± 0.0005	647 ± 19
280	169 ± 14	0.0123 ± 0.0010	824 ± 40
310	209 ± 12	0.0118 ± 0.0007	838 ± 22
130 and 310	174 ± 20	0.0102 ± 0.0014	718 ± 48

the minimum of the well, and it was determined that the least squares values rose monotonically with change in C_0 and C_1 above 4.5% of the minimum value of each well. The analysis also revealed that the C_0 and C_1 parameters are coupled and still yield equivalent least square fits by the simultaneous variation in C_0 and C_1 values. Therefore, the error values for C_0 and C_1 reported in Table I represent the range of simultaneous changes in C_0 and C_1 values that meet the criteria of having least square values less than 4.5% above the well minimum. Although the coupling of the fit C_0 and C_1 values indicates that there is some uncertainty in the internal energy dependence of the $C_6H_6^*$ CET, this results in less than a 5% change in all of the $\alpha_1(E')$ values at $E' = 53\,326\ cm^{-1}$. Also, the lowest and highest ΔT temperature rises (130 K and 310 K) were fit simultaneously to obtain a temperature independent set of parameters, which are also included in Table I. This fit falls within the 2σ error bars of the time dependent temperature values of the lowest and highest ΔT temperature rises, but falls outside many of the 1σ time dependent temperature error bars.

Since the bath temperature does not change during simulations in the MultiWell program, the $\alpha_1(E')$ values did not change due to parameters affected by bath temperature changes during the simulation. However, since the bath temperature does change in the experimental data, the optimized parameters we report for $\alpha_1(E')$ represent a combination of two factors that influence the CET efficiency: bath temperature and internal energy of benzene. We therefore plotted $-\langle \Delta E\rangle$ as a function of $\langle E'\rangle$ generated from optimized fits of time-dependent temperature rises corresponding to various final temperatures, Figure 8, in order to estimate the effect of temperature on the CET rate efficiency. Figure 8 shows that the magnitude of $\langle \Delta E\rangle$ increases with both $\langle E'\rangle$ and final bath temperature. Data from Yerram *et al.*: $C_6H_6^*$ –N_2 and $C_6H_6^*$ –C_6H_6 IRF CET measurements are also reproduced in Figure 8.[41] Our experimental $C_6H_6^*$ –N_2 $\langle \Delta E\rangle$ data are larger in magnitude than the $C_6H_6^*$ –N_2 IRF data and smaller in magnitude than the $C_6H_6^*$ –C_6H_6 IRF data for all $\langle E'\rangle$ values. However, since the magnitude of our $\langle \Delta E\rangle$ data decreases with decreasing final bath temperature, we also generated an extrapolation to the $-\langle \Delta E\rangle$ vs $\langle E'\rangle$ curve that we would expect from a $\Delta T = 0$ K experiment. The extrapolated curve was made by linearly fitting the optimized C_0 and C_1 parameters as a function of ΔT and then running a MultiWell simulation with the $\Delta T = 0$ K extrapolated C_0 and C_1 values. The extrapolated $-\langle \Delta E\rangle$ vs $\langle E'\rangle$ curve is in very good agreement with the $C_6H_6^*$ –N_2 IRF data, falling within the error bars of that data for most reported $\langle E'\rangle$ values. Also, given the CET rate dependence on bath temperature that we observe, it is to be expected that our experimental $C_6H_6^*$ –N_2 $-\langle \Delta E\rangle$ data are larger than the $C_6H_6^*$ –N_2 IRF data since the IRF CET data were collected in a dilute enough mixture to cause negligible rise in bath temperature.

Fits to recent classical trajectory calculations of $C_6F_6^*$ –N_2 and "model" $C_6H_6^*$ –N_2 CET by Paul *et al.* are also included in Figure 8.[6,7] The simulations were carried out in a regime in which the rise in bath temperature during the simulation is <10 K and therefore the CET efficiency was not significantly affected by changes in bath temperature. The simulations also represent the regime in which there

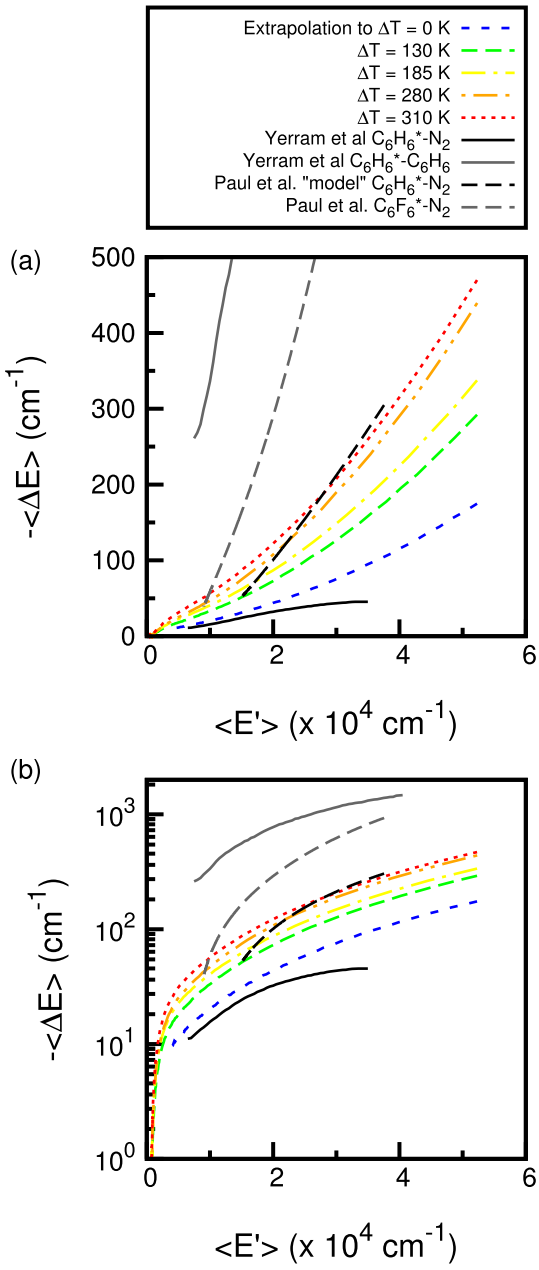

FIG. 8. (a) Average energy transferred per collision vs. average vibrational energy of $C_6H_6^*$ for models of temperature-binned temperature rises. (b) log plot of (a). Our experimental data were plotted alongside reconstructed IRF data adapted with permission from Yerram *et al.*, J. Phys. Chem. **94**, 6341 (1990). Copyright 1990 American Chemical Society, as well as fit curves to simulations adapted with permission from A. K. Paul, S. C. Kohale, and W. L. Hase, J. Phys. Chem. C. **119**, 14683 (2015). Copyright 2015 American Chemical Society.

is no $C_6F_6^*$ –C_6F_6 or $C_6H_6^*$ –C_6H_6 CET since they were carried out with only one C_6F_6 or C_6H_6 molecule in a N_2 bath. The $C_6F_6^*$ –N_2 $\langle \Delta E\rangle$ values that the authors obtained is larger than the $\langle \Delta E\rangle$ values predicted by extrapolation of our $C_6H_6^*$ –N_2 $\langle \Delta E\rangle$ data to $\Delta T = 0$ K as expected. Previous work has demonstrated that C_6F_6 CET is more efficient than C_6H_6 CET largely due to the decrease in vibrational frequencies as well as increase in steepness of the repulsive region of the intermolecular potentials upon fluorination of benzene.[1] The "model" $C_6H_6^*$ –N_2 $\langle \Delta E\rangle$ values are also larger than the $\langle \Delta E\rangle$ values predicted by

the extrapolation of our $C_6H_6^*$ –$N_2\langle\Delta E\rangle$ data to $\Delta T = 0$ K. The "model C_6H_6" utilized C_6H_6 atomic masses but retained the C_6F_6 intermolecular potentials. Utilization of C_6H_6 atomic masses decreased the CET efficiency due to an increase in vibrational frequencies which has been shown to decrease CET efficiency in other studies.[1,4] However, utilization of C_6F_6 –N_2 intermolecular potentials resulted in an increase in CET as compared to C_6H_6 –N_2 intermolecular potentials since C_6F_6 –N_2 intermolecular potentials have a steeper repulsive wall which has been shown to increase CET efficiency in impulsive collisions.[1,70] Furthermore, unpublished results from the calculation of "real" $C_6H_6^*$ –N_2 CET by Paul *et al.* utilizing C_6H_6 atomic masses, intramolecular potentials, and intermolecular potentials yielded $\langle\Delta E\rangle$ values that are lower than "model" $C_6H_6^*$ –$N_2\langle\Delta E\rangle$ values.[71]

Measurements by Yerram *et al.* of $C_6H_6^*$ –N_2 and $C_6H_6^*$ –Ar IRF CET also suggest that CET efficiency is similar in magnitude throughout the relaxation of benzene.[41] In work by Lenzer *et al.*, $C_6H_6^*$ –Ar $\langle\Delta E\rangle$ was approximately −50 cm^{-1} for bath temperature of 300 K with an $\langle E'\rangle$ of 40 700 cm^{-1}.[1] This value is consistent with an extrapolation of Yerram *et al.* $C_6H_6^*$ –$N_2\langle\Delta E\rangle$ values in Figure 8. In classical trajectory calculations by Bernshtein *et al.*, $C_6H_6^*$ –Ar $\langle\Delta E\rangle$ values were −44 cm^{-1} and −53 cm^{-1} for bath temperatures of 300 K and 500 K given an $\langle E'\rangle$ of 40 700 cm^{-1}.[32] This is a 20% increase in $C_6H_6^*$ –Ar CET efficiency when the bath temperature is increased from 300 K to 500 K which is consistent with the trend we observe in $C_6H_6^*$ –N_2 CET. The authors also determined that $C_6H_6^*$ –$C_6H_6\langle\Delta E\rangle$ values were −755 cm^{-1} and −713 cm^{-1} for bath temperatures of 300 K and 500 K respectively given an $\langle E'\rangle$ of 40 700 cm^{-1}.[32] This is a 5.6% decrease in $C_6H_6^*$ –C_6H_6 CET efficiency when the bath temperature is increased from 300 K to 500 K indicating that the total energy transfer from excited benzene to unexcited benzene becomes less significant at higher temperatures.

Since the average initial energy transferred from a deactivating collision, $\langle\Delta E_d\rangle$ in Equation (8), is often reported in studies utilizing a master equation treatment as well as in CET studies, we report a plot of $\langle\Delta E_d\rangle$ values versus final temperature of the temperature rise in Figure 9. To generate this figure, the parameters in Table I were utilized for the P_{down} equation, Equation (6), when calculating the $\langle\Delta E_d\rangle$ values at the assumed $\langle E'\rangle$ value of 51 813 cm^{-1}. Therefore the $\langle\Delta E_d\rangle$ values we present in Figure 9 are from collisions from nascent 193 nm photoexcited benzene to a bath at the extrapolated initial temperature values between 400 and 650 K.

The extrapolated value of $\langle\Delta E_d\rangle$ that we predict at 300 K is 354 cm^{-1} which is smaller than the value of 400 cm^{-1} utilized by Miller and Klippenstein at 300 K.[60] However, our $\langle\Delta E_d\rangle$ fit increases more quickly with temperature than the model employed by Miller and Klippenstein.[60] It is also important to note that Miller *et al.* did not utilize an internal energy dependence in their CET rate modeling. For comparison to classical trajectory calculations by Bernshtein *et al.*, we also generated the fit of our $\langle\Delta E_d\rangle$ values, $\langle\Delta E_d\rangle = 300*(T_{final}/300)^{1.12}$ cm^{-1}, given an $\langle E'\rangle$ of 40 700 cm^{-1}.[32] Bernshtein *et al.* reported $C_6H_6^*$ –Ar $\langle\Delta E_d\rangle$ values of 182 cm^{-1} and 249 cm^{-1} for bath temperatures of 300 K and 500 K, respectively, given an initial benzene $\langle E'\rangle$ of 40 700 cm^{-1} in classical trajectory calculations. This corresponds to a 36% increase in $C_6H_6^*$ –Ar $\langle\Delta E_d\rangle$ when the bath temperature is increased from 300 K to 500 K which is consistent with the trend we see in $C_6H_6^*$ –N_2 CET. However, the $C_6H_6^*$ –Ar $\langle\Delta E_d\rangle$ is substantially lower than the $C_6H_6^*$ –$N_2\langle\Delta E_d\rangle$ of 300 cm^{-1} obtained from extrapolating our fit to 300 K given an $\langle E'\rangle$ of 40 700 cm^{-1}.

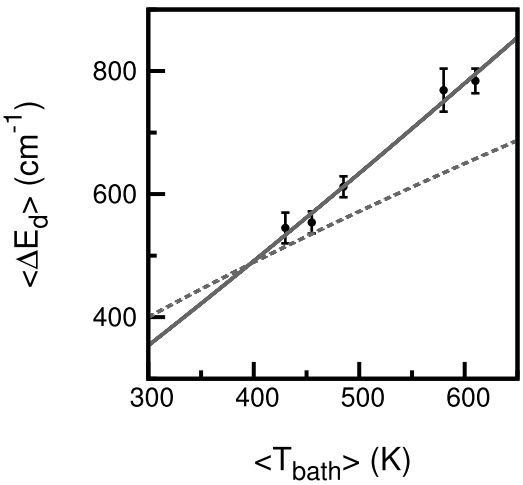

FIG. 9. Initial $\langle\Delta E_d\rangle$ values (black circles) for temperature rises to given average final temperatures between 3 and 6 μs and fit equation $\langle\Delta E_d\rangle = 354*(T_{final}/300)^{1.14}$ cm^{-1} (solid grey line). Error bars represent error in $\alpha_1(E')$ values in Table I. Also plotted is the temperature dependent $\langle\Delta E_d\rangle$ utilized by Miller and Klippenstein, $\langle\Delta E_d\rangle = 400*(T_{final}/300)^{0.7}$ cm^{-1} (dashed grey line).[60]

IV. CONCLUSIONS

The time-dependent temperature rise of a N_2 bath was measured in order to investigate the V-RT CET behavior of highly vibrationally excited benzene colliding with N_2 bath molecules. We observed a clear increase in rate of the experimental temperature rise with increase in final bath temperature which could not be described using a CET dependency on either the bath temperature or the internal excitation of benzene independently. We find that the best fit model of the CET depended linearly on the internal energy of the excited benzene molecules as well as depended approximately linearly on the temperature of the N_2 bath.

The V-RT CET behavior measured in this paper is consistent with previous excited benzene CET experiments and calculations.[6,7,41] In numerous previous studies, the CET efficiency is modeled as increasing with increase in internal excitation as well as increasing with increase in bath temperature which is consistent with our results. In our analysis, we have neglected the effect of a number of CET processes in temperature rise modeling including $C_6H_6^*$ –C_6H_6 CET and supercollisions. It is possible that $C_6H_6^*$ –C_6H_6 CET affects the rate of bath temperature rise, but $C_6H_6^*$ –C_6H_6 collisions are suspected to play a minor role in the prediction of CET to the bath in this experiment. In addition, the role of supercollisions in generating metastable highly rotationally excited N_2 is suspected to cause the energy transfer to the bath to be underestimated in our modeling. The effect of this small percentage of collisions is also suspected to increase with increase in temperature.[32] Ultimately, we believe that our model temperature

rises provide a good estimate of the CET processes for >95% of the temperature rise in the bath although there may be slower CET processes that would cause our model to underestimate the total energy transferred from highly vibrationally excited benzene to the rotation-translation modes of the N_2 bath.

In future work, we plan to extend these experiments to lower initial temperatures between 34 and 120 K via pulsed converging-diverging nozzle gas expansion.[72] There are very few studies that have examined CET dependencies on internal energy of highly vibrationally excited aromatic molecules as well as on bath temperature at this range of temperatures. We anticipate that V-RT CET efficiency will continue to decrease at lower temperatures in accordance with the impulsive collision model and that V-V CET efficiency will dramatically increase at lower temperatures due to the increasing importance of long range interactions in CET at lower temperatures.[31]

ACKNOWLEDGMENTS

Funding for this project was provided by the United States Air Force Office of Research (Grant No. C13-0027). The authors would like to thank Dr. W. L. Hase and Dr. A. K. Paul for helpful discussions. The authors want to acknowledge the Texas A&M University Machine Shop. The authors also want to acknowledge Dr. Lisa M. Pérez for valuable discussion and the Laboratory for Molecular Simulation at Texas A&M University for providing computing resources.

[1]T. Lenzer, K. Luther, J. Troe, R. G. Gilbert, and K. F. Lim, J. Chem. Phys. **103**, 626 (1995).
[2]J. D. Brenner, J. P. Erinjeri, and J. R. Barker, Chem. Phys. **175**, 99 (1993).
[3]A. J. Sedlacek, R. E. Weston, and G. W. Flynn, J. Chem. Phys. **94**, 6483 (1991).
[4]D. G. Mitchell, A. M. Johnson, J. A. Johnson, K. A. Judd, K. Kim, M. Mayhew, A. L. Powell, and E. T. Sevy, J. Phys. Chem. A **112**, 1157 (2008).
[5]C. A. Michaels, Z. Lin, A. S. Mullin, H. C. Tapalian, and G. W. Flynn, J. Chem. Phys. **106**, 7055 (1997).
[6]A. K. Paul, S. C. Kohale, and W. L. Hase, J. Phys. Chem. C **119**, 14683 (2015).
[7]A. K. Paul, S. C. Kohale, S. Pratihar, R. Sun, S. W. North, and W. L. Hase, J. Chem. Phys. **140**(19), 194103 (2014).
[8]N. Nakashima and K. Yoshihara, J. Phys. Chem. **93**, 7763 (1989).
[9]L. Brouwer, H. Hippler, L. Lindemann, and J. Troe, J. Phys. Chem. **89**, 4608 (1985).
[10]C.-L. Liu, H. C. Hsu, Y. C. Hsu, and C.-K. Ni, J. Chem. Phys. **127**, 104311 (2007).
[11]H. Hippler, K. Luther, J. Troe, and H. Wendelken, J. Chem. Phys. **79**, 239 (1983).
[12]D. K. Havey, J. A. Du, Q. N. Liu, and A. S. Mullin, J. Phys. Chem. A **114**, 1569 (2010).
[13]J. Du, N. A. Sassin, D. K. Hayey, K. L. Hsu, and A. S. Mullin, J. Phys. Chem. A **117**, 12104 (2013).
[14]Z. M. Li, R. Sansom, S. Bonella, D. F. Coker, and A. S. Mullin, J. Phys. Chem. A **109**, 7657 (2005).
[15]S. T. Tsai, C. K. Lin, Y. T. Lee, and C. K. Ni, J. Chem. Phys. **113**, 67 (2000).
[16]N. Nakashima and K. Yoshihara, J. Chem. Phys. **79**, 2727 (1983).
[17]M. Klessinger and J. Michl, *Excited States and Photochemistry of Organic Molecules* (VCH, New York, 1995).
[18]C. E. Otis, J. L. Knee, and P. M. Johnson, J. Chem. Phys. **78**, 2091 (1983).
[19]M. Sumitani, D. V. Oconnor, Y. Takagi, N. Nakashima, K. Kamogawa, Y. Udagawa, and K. Yoshihara, Chem. Phys. **93**, 359 (1985).
[20]M. A. Duncan, T. G. Dietz, M. G. Liverman, and R. E. Smalley, J. Phys. Chem. **85**, 7 (1981).
[21]J. K. Foote, M. H. Mallon, and J. N. Pitts, J. Am. Chem. Soc. **88**, 3698 (1966).
[22]K. Shindo and S. Lipsky, J. Chem. Phys. **45**, 2292 (1966).
[23]J. P. Reilly and K. L. Kompa, J. Chem. Phys. **73**, 5468 (1980).
[24]A. Yokoyama, X. Zhao, E. J. Hintsa, R. E. Continetti, and Y. T. Lee, J. Chem. Phys. **92**, 4222 (1990).
[25]T. C. Hsu, J. N. Shu, Y. Chen, J. J. Lin, Y. T. Lee, and X. M. Yang, J. Chin. Chem. Soc. **49**, 1 (2002).
[26]V. V. Kislov, T. L. Nguyen, A. M. Mebel, S. H. Lin, and S. C. Smith, J. Chem. Phys. **120**, 7008 (2004).
[27]S. Y. Toh, P. Djuricanin, T. Momose, and J. Miyazaki, J. Phys. Chem. A **119**, 2683 (2015).
[28]T. C. Hsu, J. N. Shu, Y. Chen, J. J. Lin, Y. T. Lee, and X. M. Yang, J. Chem. Phys. **115**, 9623 (2001).
[29]J. R. Barker, Int. J. Chem. Kinet. **33**, 232 (2001).
[30]J. R. Barker, Int. J. Chem. Kinet. **41**, 748 (2009).
[31]J. R. Barker, L. M. Yoder, and K. D. King, J. Phys. Chem. A **105**, 796 (2001).
[32]V. Bernshtein and I. Oref, J. Phys. Chem. B **109**, 8310 (2005).
[33]G. P. Smith and J. R. Barker, Chem. Phys. Lett. **78**, 253 (1981).
[34]M. J. Rossi and J. R. Barker, Chem. Phys. Lett. **85**, 21 (1982).
[35]M. J. Rossi, J. R. Pladziewicz, and J. R. Barker, J. Chem. Phys. **78**, 6695 (1983).
[36]T. Ichimura, Y. Mori, N. Nakashima, and K. Yoshihara, Chem. Phys. Lett. **104**, 533 (1984).
[37]T. Ichimura, Y. Mori, N. Nakashima, and K. Yoshihara, J. Chem. Phys. **83**, 117 (1985).
[38]T. Ichimura, M. Takahashi, and Y. Mori, Chem. Phys. **114**, 111 (1987).
[39]N. Nakashima, H. Inoue, M. Sumitani, and K. Yoshihara, J. Chem. Phys. **73**, 5976 (1980).
[40]N. Nakashima and K. Yoshihara, J. Chem. Phys. **77**, 6040 (1982).
[41]M. L. Yerram, J. D. Brenner, K. D. King, and J. R. Barker, J. Phys. Chem. **94**, 6341 (1990).
[42]U. Hold, T. Lenzer, K. Luther, K. Reihs, and A. C. Symonds, J. Chem. Phys. **112**, 4076 (2000).
[43]T. Lenzer, K. Luther, K. Reihs, and A. C. Symonds, J. Chem. Phys. **112**, 4090 (2000).
[44]U. Hold, T. Lenzer, K. Luther, and A. C. Symonds, J. Chem. Phys. **119**, 11192 (2003).
[45]N. J. Brown and J. A. Miller, J. Chem. Phys. **80**, 5568 (1984).
[46]V. Bernshtein and I. Oref, J. Phys. Chem. **98**, 3782 (1994).
[47]A. Pashutski and I. Oref, J. Phys. Chem. **92**, 178 (1988).
[48]S. Hassoon, I. Oref, and C. Steel, J. Chem. Phys. **89**, 1743 (1988).
[49]J. M. Morgulis, S. S. Sapers, C. Steel, and I. Oref, J. Chem. Phys. **90**, 923 (1989).
[50]K. Luther and K. Reihs, Ber. Bunsen-Ges. Phys. Chem. **92**, 442 (1988).
[51]H. G. Lohmannsroben and K. Luther, Chem. Phys. Lett. **144**, 473 (1988).
[52]D. F. Kelley, T. Kasai, and B. S. Rabinovitch, J. Phys. Chem. **85**, 1100 (1981).
[53]R. Arakawa, D. F. Kelley, and B. S. Rabinovitch, J. Chem. Phys. **76**, 2384 (1982).
[54]A. S. Mullin, J. Park, J. Z. Chou, G. W. Flynn, and R. E. Weston, Chem. Phys. **175**, 53 (1993).
[55]G. Lendvay and G. C. Schatz, J. Phys. Chem. **94**, 8864 (1990).
[56]D. L. Clarke, K. C. Thompson, and R. G. Gilbert, Chem. Phys. Lett. **182**, 357 (1991).
[57]D. C. Clary, R. G. Gilbert, V. Bernshtein, and I. Oref, Faraday Discuss. **102**, 423 (1995).
[58]J. A. Miller, S. J. Klippenstein, and C. Raffy, J. Phys. Chem. A **106**, 4904 (2002).
[59]L. A. Miller, C. D. Cook, and J. R. Barker, J. Chem. Phys. **105**, 3012 (1996).
[60]J. A. Miller and S. J. Klippenstein, J. Phys. Chem. A **107**, 7783 (2003).
[61]A. Bolovinos, J. Philis, E. Pantos, P. Tsekeris, and G. Andritsopoulos, J. Mol. Spectrosc. **94**, 55 (1982).
[62]J. Philis, A. Bolovinos, G. Andritsopoulos, E. Pantos, and P. Tsekeris, J. Phys. B: At. Mol. Phys. **14**, 3621 (1981).
[63]J. Luque and D. Crosley, SRI International Report MP 99, 1999.
[64]R. C. Reid, J. M. Prausnitz, and B. E. Poling, *The Properties of Gases and Liquids, 4th ed.* (McGraw-Hill, New York, 1987).
[65]H. Hippler, J. Troe, and H. J. Wendelken, J. Chem. Phys. **78**, 6709 (1983).
[66]S. E. Stein and B. S. Rabinovitch, J. Chem. Phys. **58**, 2438 (1973).
[67]T. Beyer and D. F. Swinehart, Commun. ACM **16**, 379 (1973).
[68]G. Herzberg, *Molecular spectra and molecular structure. Vol. 3: Electronic spectra and electronic structure of polyatomic molecules* (Van Nostrand Reinhold Company, 450 West 33rd Street, New York, NY 10001, 1966), Vol. 3.
[69]S. Hay, F. Shokoohi, S. Callister, and C. Wittig, Chem. Phys. Lett. **118**, 6 (1985).
[70]P. D. Claire and W. L. Hase, J. Phys. Chem. **100**, 8190 (1996).
[71]A. K. Paul and W. L. Hase, unpublished results.
[72]R. Sanchez-Gonzalez, R. Srinivasan, J. Hofferth, D. Y. Kim, A. J. Tindall, R. D. W. Bowersox, and S. W. North, AIAA J. **50**, 691 (2012).